Study of a concert harp's radiation using acoustic imaging methods

Quentin Leclere[a], Jean-Loic Le Carrou[b] and François Gautier[b]

[a]Laboratoire Vibrations Acoustique - INSA Lyon, 25 bis avenue Jean Capelle, Bâtiment Saint-Exupéry, F-69621 Villeurbanne cedex, France
[b]Laboratoire d'Acoustique de l'Université du Maine, Avenue Olivier Messiaen, 72085 Le Mans, France
quentin.leclere@insa-lyon.fr

Recent studies have been conducted to understand the low frequency radiation of a concert harp. Experiments have been carried out in a semi-anechoic room: the harp's soundboard is excited with a shaker and the pressure is measured at more than 600 positions on a nearly hemispherical surface at a distance of about 2 meters from the instrument. Simple source models with a set of monopoles have been optimized to fit the measured acoustic radiation. These models are very satisfactory in the low frequency domain but cannot properly reproduce the measured field above 350Hz. The aim of this paper is to present the application of acoustic imaging tools to this academic case: volumetric velocity and acoustic power maps in the harp plane are computed with an optimized beamforming and with a regularized inverse FRF method (iFRF) up to 1kHz. The optimization of the beamforming is realized using a variable windowing factor, and the regularization of the inverse FRF method with a Tikhonov approach. The presented results show the superiority of iFRF over beamforming for this application in the whole frequency range of interest. iFRF results confirm outputs from a simple 2-monopoles model below 400Hz, and explain the reason why this simple equivalent source fails above this frequency.

1   Introduction

The concert harp is a complex sound radiator involving couplings between a flat panel, the soundboard and a cavity with 5 sound holes, the soundbox. In a previous paper [1], the vibroacoustic behavior of the concert harp was investigated in the low frequency range. The study shows the importance of two coupled modes both involving air motions inside the holes and the bending motion of the soundboard in the response of the instrument. A radiation model based on simple sources located on the soundboard and on the sound holes shows that this particular vibroacoustic behavior can also be identified [2]. However, these two studies are limited in the low frequency range (below 200 Hz). The aim of this paper is to better understand the vibro-acoustic behavior of the concert harp in the frequency range [100 Hz - 1000 Hz] by studying its acoustic radiation. To do so, two different acoustic imaging techniques are confronted: the beamforming and the inverse FRF.

After a description of the experimental setup, we summarize previous results obtained by Equivalent Sources Method (ESM), using simple sources to describe the acoustical radiation of the instrument. Then, two imaging techniques are explained (sec.4) and applied in order to be compared leading us to the identification of acoustical sources of the concert harp in a large frequency range (sec.5).

2   Experimental setup

The directivity of the sound radiated by a concert harp (*Camac Harps, Atlantide Prestige model*) is measured in a semi-anechoic room, of working volume 1000 m^3 and of valid frequency range of [20 Hz - 20 KHz]. In Figure 1 is shown a schematic diagram of the measurement set-up.

The instrument is excited by a shaker driven by a white noise connected via a rod to the back of the soundboard. The acoustic pressure is measured by 35 $\frac{1}{4}$-inch ICP microphones arranged around the harp on a fixed arch. In order to obtain the sound field in all directions, a system has been set to rotate the harp with the shaker in eighteen 10 degree steps around the z-axis. Note that only a semi-circle rotation is sufficient to obtain the sound field on the whole circle. The arch dimensions are 4.70 m in width and 3.55 m in height, enabling the positioning of microphones at a distance of 2.35 m from the rotation axis and of 0.2 m from each other along the z-axis. The 34×18+1 measurement mesh obtained with this experimental setup is a compromise between a good

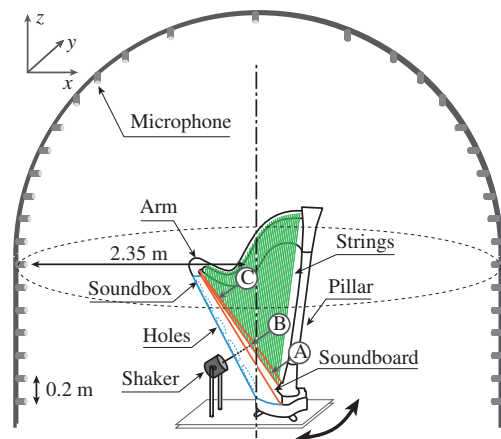graphical resolution of the sound field and technical restrictions.

Figure 1: Experimental set-up.

The force is applied by the shaker between strings 30 and 31 (respective fundamental frequencies at 138.6 Hz and 123.5 Hz), and measured by an appropriate force transducer. Therefore, for each microphone i, the frequency response function $H_i = P_i/F$ is measured.

3   Results of equivalent sources using few dofs

In this section, we present results obtained by the Equivalent Sources Method (ESM) [3]. This method consists in expressing the acoustic field as the superposition of elementary fields generated by a distribution of equivalent acoustic monopoles located inside the volume of the actual source. In our case, virtual sources have to be added to take into account the reflexive floor of the semi-anechoic room.

According to the ESM, the radiated pressure at N points can be written in a matrix form as follows (for a given frequency ω that is implicit in all the following) :

$$\{p\}_N = [H]_{N*n}\{q\}_n \tag{1}$$

where $\{p\}_N$ are acoustic pressure at microphone positions tiled in column, $\{q\}_n$ are monopole's volumetric velocities, and $[H]_{Nn}$ matrix of acoustic transfer functions, each entry being given by

$$H = j\rho\omega \left(\frac{e^{-jkr}}{4\pi r} + R\frac{e^{-jk\overline{r}}}{4\pi \overline{r}} \right) \tag{2}$$

with r and $\bar{r}$ for respectively source/receiver and image-source/receiver distances. R corresponds to the reflection coefficient of the room's floor.

Assuming that the locations of the equivalent sources are known, the volume velocity $\{q\}$ can be estimated using

$$\{q\} = [H]^+\{p\} \tag{3}$$

This equation (3) corresponds to the optimum solution in the least squares sense where $[H]^+$ is the Moore-Penrose generalized inverse of $[H]$. In the general case, positions and the volume velocities of the model are unknown. In order to find optimal values of these parameters, the relative error between the pressure field measured and the model pressure at the same point

$$\epsilon = \frac{\|\{p\} - [H]\{q\}\|^2}{\|\{p\}\|^2}, \tag{4}$$

has to be minimized. This minimization is a non-linear problem which has to be solved iteratively. Starting from initial values of the parameters, and assuming that the error function is convex in the vicinity of these initial values, optimum values are computed using a gradient technique.

Applied to a one monopole model, results show that the monopole is found on the symmetric plane of the concert harp: in the strings plane. However, this model does not represent the physical properties of the instrument since, for some frequencies, the monopole location is found outside the object. A second model based on two monopoles is found to be more adapted to the presence of the two main radiated sources: the soundboard and the sound holes. For this model, a simplified minimization procedure was applied based on physical properties: each monopole was restricted either on the soundboard or on the sound holes. The computed relative error is shown in figure 1. Results of this model show that the volume velocities associated to each source reach their maximum values for the two particular vibroacoustic modes [2]. Moreover, the phase relationship between these two monopoles is found to be characteristics of the vibroacoustic behavior of the concert harp [1, 4].

The main drawback of this method is that it is limited in low frequencies. For better understanding of the vibroacoustic behavior of the instrument, other acoustic imaging techniques have to be applied.

4 Presentation of used imaging techniques

Several methods are available to 'image' an acoustic source. In this particular case, microphones are at a quite in the far field of the source (at about 2 meters), and the microphone mesh is not adapted for techniques based on 2D DFT approaches (classical NAH [5]). The beamforming (initiated by [6]) is quite adapted to the geometry of the problem, but the resolution is the frequency range of interest (100Hz 1kHz) is known to be limited. This method is however implemented first, using an original procedure to optimize window factors. Other methods are inverse FRF approaches, like IBEM

([7]) if FRFs are computed using BEM (boundary element methods) solvers. But in this case, a fine mesh of the source's surface is required, as well as a precise positioning of the source relatively to microphones. We choose in this paper to use an alternative IFRF method based on monopole distributions to identify equivalent sources ([8], [9]). The radiation pattern of the instrument is assumed to be symmetric in the frequency range of interest. Thus, a monopole distribution is placed in the symmetry plane of the source, and volumetric velocities are identified inversing the acoustic radiation operator computed between monopoles and microphones.

4.1 beamforming

The beamforming has bean introduced by [6] as the acoustic telescope. The principle is to process microphone signals with adequate time delays to obtain constructive or destructive interferences for acoustic waves coming from one particular direction, or one particular point. The operation can be realized for a given solid angle (or for a given plane) to obtain an image of the source. In fact, each point of the resulting map is treated independently from others, as it was the unique source. The procedure is thus a scalar identification, particularly robust. The beamforming computation can be written in a matrix form :

$$\{q\}_\alpha = [H_\alpha^{-1}]^T\{p\} \tag{5}$$

with $\{p(\omega)\}$ complex values of acoustic pressures measured at pulsation ω tiled in column, $\{q(\omega)\}_{bf}$ resulting source strengths, with subscript bf for beamforming, α real positive or null, and $[H_\alpha^{-1}]^T$ the alpha-weighted transfer matrix inverted term to term and transposed, each entry of which being given by equation 2 with a reflexion coefficient $R = 0$ to avoid reflexion artifacts on the image :

$$H_\alpha = r^\alpha j\rho\omega \frac{e^{-jkr}}{4\pi r}$$

r denoting the source-receiver distance.

The windowing factor r^α is here to give more importance in the summation process to microphones that are close to a considered source point. Beamforming is not a quantitative approach. The resulting source distribution can however be corrected regarding computed average quadratic pressures at microphone positions :

$$\{q\}_\alpha^{sc} = \frac{\|\{p\}\|}{\|[H_0]\{q\}_\alpha\|}\{q\}_\alpha \tag{6}$$

with $[H_0]$ the acoustic transfer matrix without windowing factor ($\alpha = 0$) and potentially with a reflexion coefficient.

The parameter α of the windowing term can be adjusted so as to minimize the residue, i.e. the difference between measured and computed acoustic pressures :

Find α minimizing $\|[H_0]\{q\}_\alpha^{sc} - \{p\}\|$

that can be seen as the best value of α in the least square sense.

4.2 Inverse FRF

The inverse FRF approach is formally close to beam-forming. The difference is that the identification process is global and not scalar. Advantages are that the resolution is enhanced in low frequency and that the approach is quantitative. Drawbacks are a longer computation time and the ill-conditioned nature of the identification, requiring a precise regularization. The inverse FRF computation is expressed by :

$$\{q\} = [H]^{+\beta}\{p\} \tag{7}$$

with $[H]^{+\beta}$ the regularized pseudo-inverse :

$$[H]^{+\beta} = [H^*H + \beta I]^{-1}H^*$$

This operation is a pseudo inversion of the transfer matrix H with a Tikhonov regularization. The level of regularization β is adjusted in this work with the L-curve approach, using the maximization of the curvature function (see [10]).

5 Results

Presented methods are applied to the experimental case presented in section 2. The source plane for beamforming and iFRF is a 400-monopoles rectangular distribution in the symetry plane of the harp (see figure 4).

5.1 comparison of imaging methods and few dofs approaches

The three approaches are based on an error minimization between measured acoustic pressures and computed acoustic pressures using equivalent sources. A first comparison can be realized regarding the ability of each method to recompose the measured sound field, quantified by the normalized quadratic error expressed by equation 4. Errors obtained using the 2-monopoles result, beamforming and iFRF are drawn in figure 2.
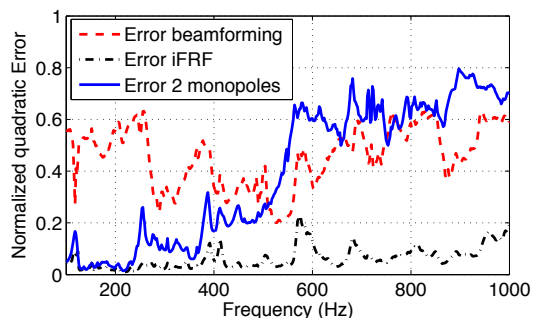

Figure 2: Quadratic error of the reconstructed pressure field using the 2 monopoles solution, beamforming and iFRF results

A first comment on figure 2 concerns the difficulty to correctly reproduce the measured pressure field using beamforming results : the normalized error using this approach varies between 20 and 60 %. This result can be explained by two things : firstly the frequency range of interest (100Hz 1kHz), too low to obtain good results,
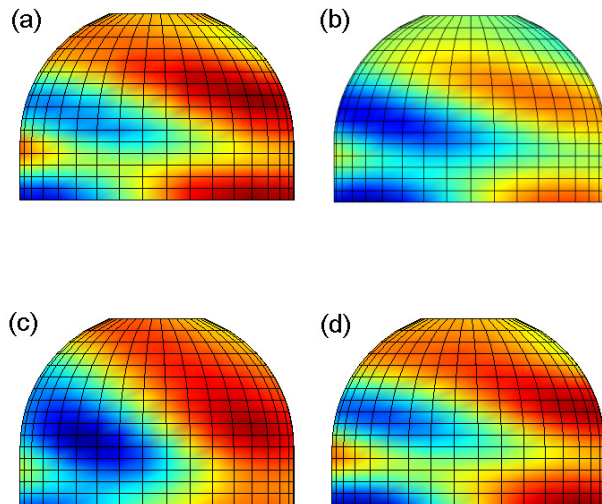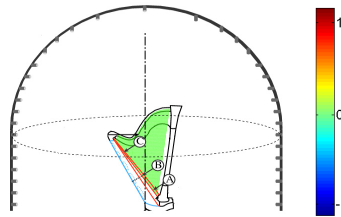

Figure 3: Real parts of the pressure fields on the microphone surface at 354 Hz (view-angle corresponding to the drawing at the top of the figure). (a) : measurements. Computed pressure fields : (b) : 2 monopoles. (c) : Beamforming. (d) : iFRF.

and secondly the 'scalar' aspect of the identification process (each source is quantified independently from the other, see section 4) that prevents beamforming to obtain real quantitative results.

The 2-monopoles approach gives good results between 100 and 400Hz, the error is less than 5% below 230Hz and less than 15% between 230 and 400Hz, except for particular frequencies for which the error can reach about 30%. Between 400 and 550 Hz the error is about 20%, and above 550Hz the error severly increases to reach 60 to 80%. This result confirms the low-frequency validity of the 2-monopoles approach, it can be expected that a 2 dofs model is no more sufficient to describe the instrument above 550Hz.

Errors obtained using the iFRF method are significantly lower than the 2-monopoles model above 230Hz. The error increases sligthly from about 3% at 100Hz to 10% at 900Hz, except for some peak values never exceeding 20%.

An example of sound field measured and computed using the three methods is given in figure 3 at 354Hz. The difficulty of beamforming to correctly recompose the sound field is also illustrated by this figure, as well as the good similarity between the measured field and iFRF results.

An interest of imaging techniques is the possibility to post process identified volumetric velocities to obtain global power maps in the whole frequency range.
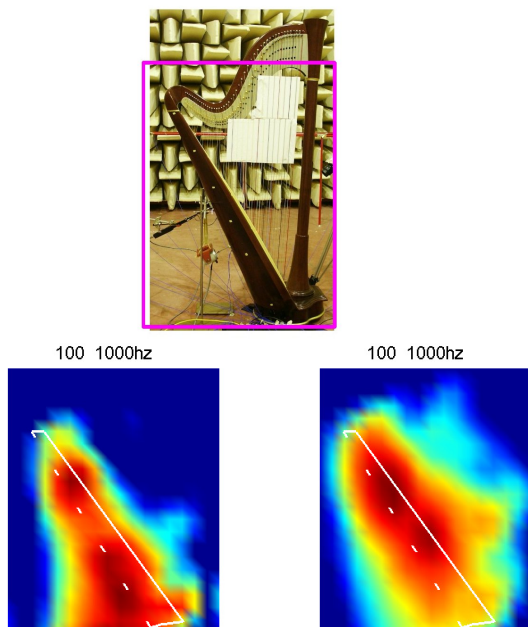
Figure 4: Top : picture of the harp and boundary (in pink) of the source plane. Acoustic power maps of the source plane by iFRF (left) and beamforming (right). Images are drawn in dB using a 10dB dynamic. The contour of the harp's soundbox with its sound holes is also shown in white.

Such maps are given in figure 4 for beamforming and iFRF, with a picture of the harp giving the delimitation of the source plane. The quality of obtained maps can be assessed by comparing the power distribution with the shape of the soundbox, which is known to be the acoustic radiator of the instrument. Both maps are presenting the acoustic power quite around the soundbox, but iFRF results seem to fit much better the soundbox than beamforming.

5.2 detailed results using Inverse FRF and the 2 monopoles model

5.2.1 Examples of volumetric velocity maps

Some single-frequency maps of volumetric velocities obtained using iFRF are given in figure 5, superimposed with results of the 2-monopoles optimization. Identified volumetric velocities are complex values, they are projected on a phase shift maximizing the quadratic energy of the map.

As shown in figure 5, the harp seems to behave as a single monopole below 400 Hz, with a position moving along the harp's body from the first hole (200Hz) to the fourth (396Hz). At 476Hz, a dipole behavior is found with an axis along the box. At 750Hz, a more complicated source is obtained, with typical phase relationships between areas corresponding to the harp's holes. The 2-monopoles model seems to fail at this frequency, by lack of source dofs.

The interpretation of such results is not straightforward. The fact that results correspond to equivalent sources has to be kept in mind, it allows to understand the far-field behavior of the acoustic source, but the real acoustic radiation mechanism is not available from
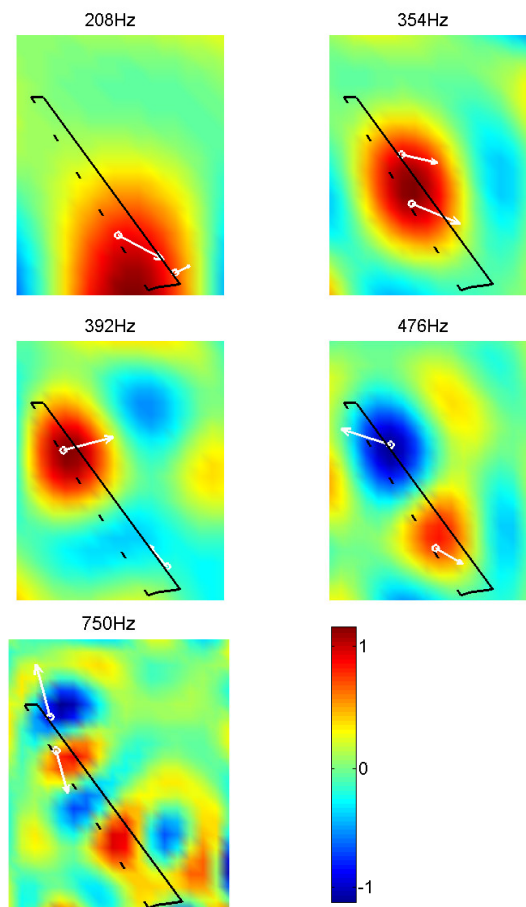

Figure 5: Examples of volumetric velocity maps for some characteristic frequencies. Maps are drawn as real quantities, for a phase shift maximizing the global quadratic energy. Amplitude and phase results of the 2-monopoles model are superimposed, arrow origins, lengths, and orientations standing respectively for monopole positions, amplitudes and phases.

such measurements. For exemple, it is found with the IFRF method that the instrument behaves as a single monopole in low frequencies. However, it is well known that the harp has two acoutical sources (soundboard and sound holes) [2]. Thus, the method can not identify each physical source in the far field. Nevertheless, result that the equivalent source of the harp radiation, obtained by the IFRF method, moves from the bottom to the top of the instrument according to the increasing of frequencies is consistent with the 2 monopoles model. An other interesting result is is that the equivalent source moves from sound hole to an other sound hole which really corresponds to the physical behavior of the system.

This kind of study has to be coupled with a modal analysis of the object to properly understand the physical phenomena leading to measured acoustic radiation patterns.

5.2.2 Evolution of the acoustic power map in function of the frequency

To complete the study it can be interesting to characterize the acoustic power maps in function of the frequency. The studied frequency range has been divided in five bands showing typical acoustic power distribu-

tions. The power maps by frequency bands are given in figure 6. Below 250 Hz, the power distribution seems
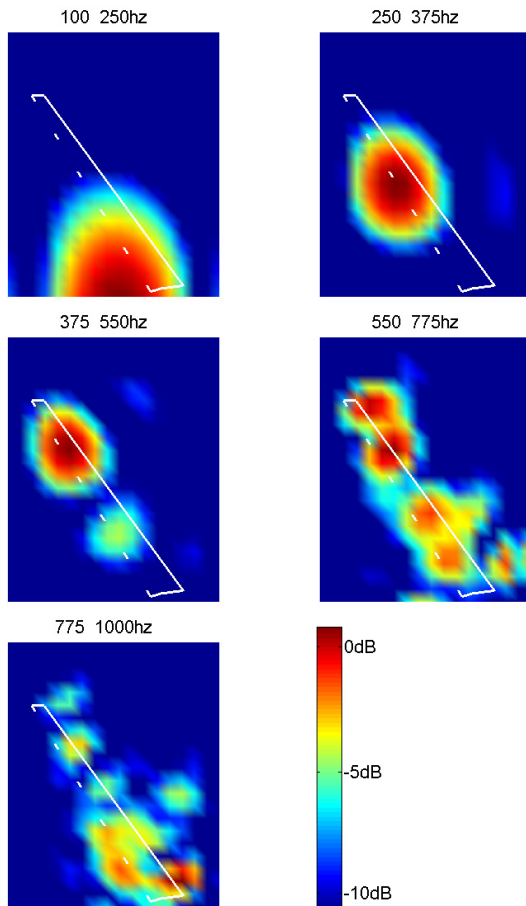

Figure 6: Acoustic power maps by frequency bands using iFRF. Images are drawn in dB using a 10dB dynamic.

to stay around the floor. This can be explained by the difficulty of the identification to 'see' the harp and its image as two separated sources. A resulting source is then obtained near the reflective surface. Between 250 and 375 Hz, the acoustic power is centered on the harp's body at the heigth of the third hole. After 375 Hz, the acoustic power moves rapidly from the third to the fourth hole, and another source appear at the heigth of the second hole. Between 550 and 775 Hz, the principal acoustic power source is located at the top of the harp's body, on the table side. In the highest frequency band, between 775 and 1000Hz, the power source seems to go down again around the first and second holes. But for this last frequency range, some ghost images appear because of the microphone mesh : the distance between microphones, of about 20cm, is too large to correctly describe the sound field, leading to potentially erroneous results.

6 Conclusion

The acoustic behavior of the harp has been studied between 100 Hz and 1kHz using 3 different methods : a 2-monopoles model and two different acoustic imaging techniques : iFRF and beamforming. Beamforming has been found to be inadequate for this application, iFRF

and the 2-monopoles model giving good results. The 2-monopoles model is however limited to the low frequency range, because of the complexity of the source above 500Hz illustrated by images provided by iFRF. iFRF Results show that, in the far field, the harp can be interpreted as a single source which moves from sound hole at the bottom to sound hole at the top of the instrument according to the frequency. This single equivalent source combine the effect of the two acoustical sources of the concert harp which are the soundboard and the sound holes. In the frequency range [476Hz-750Hz], the harp behaves as a dipole, and after as more complex distributions. The physical interpretation of these results are not straightforward because of the globalisation of effects obtained by the IFRF method. Though results are very interesting, they should be coupled with a broad band modal analysis of the instrument to finely understand the radiation mechanism of the concert harp.

References

[1] J-L. Le Carrou, F. Gautier, J. Gilbert, J.R.F. Arruda, "Low frequency model of the sound radiated by a concert harp", *In proceedings* of Forum Acusticum, Budapest, Hungary (2005)

[2] J-L. Le Carrou, F. Gautier, E. Foltête, "Experimental study of A0 and T1 modes of the concert harp", *J. Acoust. Soc. Am.* 121(1), 559-567 (2007)

[3] G.H. Koopmann, L. Song, JB Fahnline, "A method for comuting acoustic filds based on the principle of wave superposition", *J. Acoust. Soc. Am.* 86(6), 2433-2438 (1989)

[4] J-L. Le Carrou, "Vibro-acoustique de la harpe de concert (Vibroacoutics of the concert harp)", PhD thesis, Université du Maine, Le Mans, France (2006)

[5] E.G. Williams, J.D. Maynard, and E. Skudrzyk. Sound source reconstructions using a microphone array. *Journal of the Acoustical Society of America*, 68(4):340–344, 1980.

[6] J. Billingsley and R. Kinns. The acoustic telescope. *Journal of Sound and Vibration*, 48(4), 1976.

[7] A.F. Seybert, F. Martinus, and D.W. Herrin. Three experiments using the inverse bem for source identification. In *Proceedings of NOVEM 2005, Saint Raphael, France*, 2005.

[8] Q. Leclere, B. Laulagnet, and L. Polac. Application of an innovative acoustic imaging technique to assess acoustic power maps of a gasoline engine. In *proceedings of Forum Acusticum 2005, Budapest, Hungary*, 2005.

[9] Q. Leclere and B. Laulagnet. An alternative acoustic imaging technique to improve capabilities of microphone array measurements. In *Proceedings of NOVEM 2005, Saint Raphaël, France*, 2005.

[10] PC Hansen. *Regularization Tools user's manual*, 2007.